Title
Frequency-domain photon migration measurements of normal and malignant tissue optical properties in a human subject.

Journal
Applied optics, 36(1)

ISSN
1559-128X

Authors
Fishkin, JB
Coquoz, O
Anderson, ER
et al.

Publication Date
1997

DOI
10.1364/ao.36.000010

Frequency-domain photon migration measurements of normal and malignant tissue optical properties in a human subject

Joshua B. Fishkin, Olivier Coquoz, Eric R. Anderson, Matthew Brenner, and Bruce J. Tromberg

A 1-GHz multifrequency, multiwavelength frequency-domain photon migration instrument is used to measure quantitatively the optical absorption (μ_a) and effective optical scattering (μ_s') of normal and malignant tissues in a human subject. Large ellipsoidal (~10-cm major axis, ~6-cm minor axes) subcutaneous malignant lesions were compared with adjacent normal sites in the abdomen and back. Absorption coefficients recorded at 674, 811, 849, and 956 nm were used to calculate tissue hemoglobin concentration (oxyhemoglobin, deoxyhemoglobin, and total), water concentration, hemoglobin oxygen saturation, and blood volume fraction *in vivo*. Our results show that the normal and the malignant tissues measured in the patient have clearly resolvable optical and physiological property differences that may be broadly useful in identifying and characterizing tumors.

Key words: Light propagation in tissues, *in vivo*, diode lasers, near infrared, absorption, scattering, tumor, hemoglobin, water.

1. Introduction

Considerable interest has been generated in the use of optical techniques for locating, identifying, and monitoring malignant transformations. Optical methods are particularly attractive because not only do they offer the possibility of providing tissue functional information, they are relatively inexpensive and do not employ ionizing radiation. However, the precise relationship between *in vivo* optical properties and *in vivo* tissue physiology is not well understood. Extensive *in vitro* measurements of the optical properties of various tissues have been reported in the literature[1–3] but it is not clear from these studies how the optical properties of various types of biological tissue differ from each other *in vivo*. Consequently our goal is to determine quantitatively absolute optical and physiological properties of human tissues *in vivo* and correlate this information with conventional structural data derived from other sources (e.g., x-ray imaging, histopathology). Because optical properties (absolute absorption and scattering parameters) are the fundamental determinants of contrast in optical images, we believe that quantitative *in vivo* measurements are essential for realistically estimating the feasibility of optical detection of tumors.

To obtain accurate quantitative measurements of the absolute optical parameters of various types of tissue, we have constructed a portable, high-bandwidth (0.3 MHz–1 GHz), multiwavelength frequency-domain photon migration (FDPM) instrument.[4,5] The focus of our efforts in performing the frequency-domain measurements presented in this paper is to characterize normal and malignant tissue transformations encountered in a human subject. FDPM is an optical technique that can be used to determine quantitatively absolute tissue optical absorption and reduced scattering parameters in a single, noninvasive measurement. In FDPM the intensity of light incident upon an optically turbid sample is modulated at high frequencies, and the diffusely reflected or transmitted signal is measured with a phase-sensitive detector. Amplitude-modulated light propagates through multiple-scattering media with a coherent front, forming

J. B. Fishkin, O. Coquoz, M. Brenner, and B. J. Tromberg are with the Beckman Laser Institute and Medical Clinic, University of California at Irvine, 1002 Health Sciences Road East, Irvine, California 92612. E. R. Anderson is with EA Photonics, 2515 Fisk Lane, Redondo Beach, California 90278.

Received 10 May 1996; revised manuscript received 23 August 1996.

0003-6935/97/010010-11$10.00/0

photon density waves (PDW's).[6–8] PDW dispersion is highly dependent on the optical properties of the medium.[9] Thus measurements of the frequency- or distance-dependent phase and amplitude of PDW's can be used to derive absolute optical absorption and reduced scattering coefficients within a turbid medium.

In this paper we concentrate on the relationship between *in vivo* optical properties and tissue physiological parameters in a single human subject. It is not our intent to present a library of optical properties obtained from multiple human subjects, and it is unclear whether simple cataloging will provide sufficient predictive power for identifying malignancies by the use of optical imaging methods. Rather, we present a detailed study on a single patient with multiple normal and malignant sites in order to characterize a system with built-in internal controls. In this manner, we expect to gain fundamental insight into the precise nature of optical and physiological property changes that can occur in the case of malignant transformation. By obtaining individual patient information, we hope to clarify specific detectable physiological changes that can be exploited by optical diagnostic methods. Consequently we use the absolute optical properties extracted from *in vivo* FDPM measurements at multiple wavelengths to calculate hemoglobin (Hb) concentration (oxygenated, deoxygenated, and total forms), blood volume fraction (BVF) in the tissue, O_2 saturation of Hb, and H_2O concentration. Our results clearly show that tumor and normal tissue optical properties and physiological parameters measured *in vivo* differ substantially within the individual we studied.

2. Theory: Frequency-Domain Diffusion Model for a Semi-infinite Medium

Frequency-domain methods, in which the light source intensity is modulated at high frequency, have been successfully applied to *in vitro* spectroscopy studies of turbid media.[5,9–12] Analytical solutions to the frequency-domain standard diffusion equation (SDE) were employed in these studies to extract accurate absolute absorption and reduced scattering coefficient spectra from frequency-domain data acquired in turbid media. The frequency-domain SDE has been estimated to be applicable to the study of thick, turbid, macroscopically homogeneous turbid media when the source–detector separation is typically greater than 1 cm and the source modulation frequency is less than 1 GHz.[13] The frequency-domain measurements presented in this paper were noninvasively performed with the light source and the light detector placed directly on the turbid medium surface in a reflection geometry under conditions in which the SDE is applicable. We have therefore employed analytical frequency-domain SDE expressions derived by Haskell *et al.*[14] to extract absolute absorption and reduced scattering coefficients from our frequency-domain phase-shift data. These frequency-domain SDE expressions, which take into account the index of refraction mismatch at the interface between air and the turbid medium, assume that the turbid medium under study is semi-infinite in extent and macroscopically homogeneous. The equations that describe the phase shift Φ of a PDW propagating in a macroscopically homogeneous semi-infinite medium (equations 2.7.1 and 2.7.2 in the paper by Haskell *et al.*[14]) are given as

$$\Phi(\mu_a, \mu_s', \rho, \omega) = k_{\text{imag}} r_o - \arctan(\text{IMAG}/\text{REAL}), \tag{1}$$

where

$$\text{REAL} = \frac{\exp(-k_{\text{real}} r_o)}{r_o} - \cos[k_{\text{imag}}(r_{\text{ob}} - r_o)] \times \frac{\exp(-k_{\text{real}} r_{\text{ob}})}{r_{\text{ob}}}, \tag{2}$$

$$\text{IMAG} = \sin[k_{\text{imag}}(r_{\text{ob}} - r_o)] \frac{\exp(-k_{\text{real}} r_{\text{ob}})}{r_{\text{ob}}}, \tag{3}$$

$$k_{\text{real}} = \left(\frac{3}{2}\mu_a \mu_s'\right)^{1/2} \left\{\left[1 + \left(\frac{\omega}{c\mu_a}\right)^2\right]^{1/2} + 1\right\}^{1/2}, \tag{4}$$

$$k_{\text{imag}} = \left(\frac{3}{2}\mu_a \mu_s'\right)^{1/2} \left\{\left[1 + \left(\frac{\omega}{c\mu_a}\right)^2\right]^{1/2} - 1\right\}^{1/2}, \tag{5}$$

$$r_o = \left[\left(\frac{1}{\mu_s'}\right)^2 + \rho^2\right]^{1/2},$$
$$r_{\text{ob}} = \left[\left(2z_b + \frac{1}{\mu_s'}\right)^2 + \rho^2\right]^{1/2}, \tag{6}$$

$$z_b = \frac{1 + R_{\text{eff}}}{1 - R_{\text{eff}}}\left(\frac{2}{3\mu_s'}\right). \tag{7}$$

Here, μ_a is the absolute absorption coefficient in units of inverse centimeters, μ_s' is the reduced scattering coefficient in units of inverse centimeters, ρ is the distance separating the source and the detector on the surface of the turbid medium in units of centimeters, ω is the angular intensity-modulation frequency of the light source, c is the speed of light in the transporting medium surrounding the scattering particles, and R_{eff} is the effective reflection coefficient. R_{eff} (defined in equation 2.3.7 in the paper by Haskell *et al.*[14]) represents the fraction of the diffusing light in the semi-infinite turbid medium that is internally reflected because of the index of refraction mismatch at the medium boundary. Equations (1)–(7) describe an extrapolated boundary condition, which is schematically represented in Fig. 1. Z_b is the distance from the medium surface to the extrapolated boundary. We calculate R_{eff} from indices of refraction n and n_{out} (see Fig. 1 for definitions), utilizing the Fresnel reflection coefficient for unpolarized light.[14]

We use Eq. (1) to extract the absolute optical absorption coefficient μ_a and reduced scattering coefficient μ_s' from frequency-domain data acquired *in vivo*

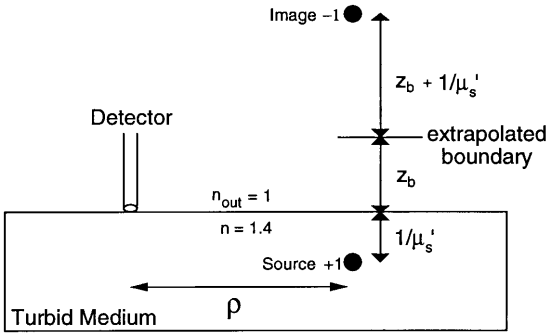

Fig. 1. Source and image configuration for the extrapolated boundary condition.[14] The placement of the image is scaled approximately for an air–medium interface, with the refractive index of the medium equal to that of tissue.[15]

in biological tissue. Our goal is to calculate *in vivo* tissue physiological properties from *in vivo* measurements of μ_a and μ_s' at multiple light source wavelengths λ and multiple source–detector separations ρ.

3. Experimental Apparatus and Method

A. Portable, Multisource, High-Bandwidth Frequency-Domain Photon Migration Instrument

A portable, multilight source, high-bandwidth, FDPM instrument is used to perform all of our measurements.[5] A network analyzer (Hewlett-Packard Model 8753C) is used to produce modulation swept from 300 kHz to 1 GHz that is superimposed on the direct current of a diode laser. Four different lasers are currently available on this instrument (SDL, Inc. Models 7421, 5420, 5421, and 6321 at 674, 811, 849, and 956 nm, respectively) and each diode is addressed serially by a rf switch. The optical power coupled into the tissue on the day of our measurements on the human subject averaged approximately 30 mW for the 674-, 811-, and 849-nm laser diodes and approximately 1 mW for the 956-nm laser diode. An avalanche photodiode (Hamamatsu Model C5658) is used to detect the diffuse optical signal that propagates through the biological tissue. A 100-μm-diameter gradient-index fiber is coupled to the light source used for tissue measurements, with the avalanche photodiode and the probe end of the source optical fiber in direct contact with the patient (i.e., a semi-infinite medium measurement geometry, Fig. 1). Measurement time depends on the precision required and the number of sweeps performed. For the measurements performed on the human subject, the time used to sweep over the 1-GHz band of modulation frequencies was 1 s. The network analyzer is controlled by a computer (Macintosh Quadra) and virtual instrument software (LABVIEW, National Instruments). The source–detector separations used for our FDPM measurements on the human subject were 1.7, 2.2, and 2.7 cm.

B. Calibration of the Frequency-Domain Apparatus

A measurement of the phase shift of intensity-modulated light at source wavelength λ propagating through a turbid medium at a given source–detector separation ρ can be expressed as

$$\Phi_{\text{measured}}(\mu_a, \mu_s', \rho, \omega) = \Phi_{\text{medium}}(\mu_a, \mu_s', \rho, \omega) + \Phi_{\text{instrument}}(\omega, \lambda), \quad (8)$$

where $\Phi_{\text{measured}}(\mu_a, \mu_s', \rho, \omega)$ is the phase shift measured at ρ at angular modulation frequency ω and source wavelength λ, $\Phi_{\text{medium}}(\mu_a, \mu_s', \rho, \omega)$ is the actual phase shift of the intensity-modulated light caused only by the medium optical properties, and $\Phi_{\text{instrument}}(\omega, \lambda)$ is the instrument phase. $\Phi_{\text{instrument}}(\omega, \lambda)$ is dependent on the properties of the light source, detector, optical fibers, and the electrical response of the phase-sensitive detection system. Because $\mu_a(\lambda)$ and $\mu_s'(\lambda)$ are the immediate quantities of interest in a FDPM measurement, an accurate determination of these optical parameters from the phase-shift data necessitates an analysis of $\Phi_{\text{medium}}(\mu_a, \mu_s', \rho, \omega)$ data rather than a direct analysis of $\Phi_{\text{measured}}(\mu_a, \mu_s', \rho, \omega)$ data. Thus we subtract $\Phi_{\text{instrument}}(\omega, \lambda)$ from $\Phi_{\text{measured}}(\mu_a, \mu_s', \rho, \omega)$ data before the data analysis in order to yield more accurate values of $\mu_a(\lambda)$ and $\mu_s'(\lambda)$ from our FDPM data fits.

One method for eliminating the instrument response from FDPM data acquired in a macroscopically homogeneous turbid medium is to compare PDW properties measured at two different source–detector separations, ρ and ρ_o. Assuming that the instrument response at a given source wavelength is constant for separate measurements at ρ and ρ_o, the behavior of the resulting FDPM data should be entirely reflective of the optical properties of the turbid medium under investigation and independent of the above-mentioned instrument response. When this two-distances measurement technique is used, Eq. (8) yields

$$\Phi_{\text{medium}}(\mu_a, \mu_s', \rho, \omega) - \Phi_{\text{medium}}(\mu_a, \mu_s', \rho_o, \omega) = \Phi_{\text{measured}}(\mu_a, \mu_s', \rho, \omega) - \Phi_{\text{measured}}(\mu_a, \mu_s', \rho_o, \omega), \quad (9)$$

where $\Phi_{\text{instrument}}(\omega, \lambda)$ has been eliminated from the measured data, thereby allowing SDE phase-shift equations to be applied directly to the resultant FDPM data. Accurate $\mu_a(\lambda)$ and $\mu_s'(\lambda)$ spectra have been obtained by Fishkin *et al*. for a macroscopically homogeneous 2.5-μM methemoglobin/1.5% Lyposyn medium; they used the frequency-domain SDE to fit FDPM data acquired with the two-distances technique.[10] Accurate absolute optical spectra of turbid media have also been acquired by Fantini *et al*., who used this same technique.[11] This approach works well under macroscopically homogeneous measurement conditions because the frequency-domain SDE assumes that $\mu_a(\lambda)$ and $\mu_s'(\lambda)$ are independent of the source–detector separation.

However, in human biological tissues, the assumption that the $\mu_a(\lambda)$ and $\mu_s'(\lambda)$ values are constant throughout the tissue is not necessarily valid. The

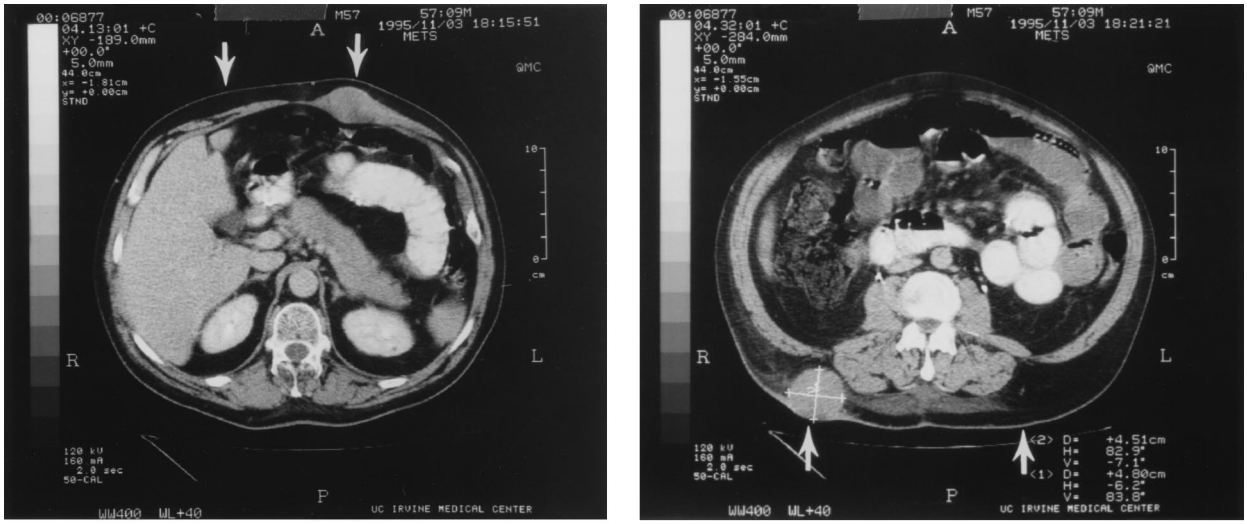

(a) (b)

Fig. 2. (a) CT scan of the subject's trunk, which was made one month before our FDPM measurements on the subject. The abdominal tumor is indicated by the right arrow (this right arrow also indicates the source–detector location for the FDPM tumor measurement). The left arrow indicates the source–detector location for the FDPM measurements on the opposite-side normal abdominal tissue. A, anterior; P, posterior; R, right; L, left. Note the distance scale (in centimeters) above the L. (b) Same as (a), except the CT scan shown here yields an image of a different cross section of the subject's trunk. The back tumor is indicated by the left arrow. The right arrow indicates the source–detector location for the FDPM measurements on the opposite-side normal back tissue.

two-distances measurement technique may compound inaccuracies inherent in applying the SDE (which assumes macroscopic homogeneity) to macroscopically heterogeneous systems. For this reason, we determine optical properties from *in vivo* FDPM data acquired at a single source–detector separation ρ. Although the application of the SDE to FDPM data acquired at a single ρ may still not be strictly accurate, we assume that the $\mu_a(\lambda)$ and $\mu_s'(\lambda)$ values measured represent an average for the heterogeneous region probed. By using this approach, we can estimate the degree of tissue heterogeneity by evaluating the optical properties at multiple values of ρ.

In order to extract $\Phi_{\text{medium}}(\mu_a, \mu_s', \rho, \omega)$ from $\Phi_{\text{measured}}(\mu_a, \mu_s', \rho, \omega)$ at a single source–detector separation ρ, $\Phi_{\text{instrument}}(\omega, \lambda)$ must be explicitly evaluated [see Eq. (8)]. We account for the contribution of $\Phi_{\text{instrument}}(\omega, \lambda)$ to $\Phi_{\text{measured}}(\mu_a, \mu_s', \rho, \omega)$ by calibrating the FDPM instrument at each λ on a macroscopically homogeneous tissuelike reference material of known optical properties. The optical properties $\mu_a(\lambda)_{\text{ref}}$ and $\mu_s'(\lambda)_{\text{ref}}$ of the homogeneous standard are obtained from FDPM data acquired with the two-distances technique. We note from Eq. (8) that the uncertainty in $\Phi_{\text{instrument}}(\omega, \lambda)$ must propagate into $\Phi_{\text{medium}}(\mu_a, \mu_s', \rho, \omega)$. The magnitude of these uncertainties has a direct impact on errors in optical and physiological property calculations.

C. Measurements on a Human Subject

We have conducted noninvasive optical property measurements of palpable tumors in a human subject. Experiments were conducted under the guidelines of the University of California at Irvine, Institutional Review Board-approved protocol 95-563. The patient was a 62-year-old white male with poorly differentiated, large-cell primary lung carcinoma. Three months after his initial staging workup, multiple subcutaneous masses began appearing over his trunk and extremities. Histological examination of needle biopsy specimens revealed poorly differentiated large-cell adenocarcinoma, similar to the primary lung cancer.

FDPM measurements were performed on two palpable subcutaneous lesions (one abdominal, one back, ellipsoidal shape with ~10-cm major axis, ~6-cm minor axes) and compared with opposite-side normal tissue. Figure 2 shows computer-aided tomography (CT) images of the subject's trunk obtained one month before the FDPM measurements. Tumors appeared to increase in size during the time interval between CT and FDPM scans. The patient received oral and intravenous iodine-based contrast agents for this CT scan. The Fig. 2(a) CT image shows the abdominal tumor measurement site, indicated by the right arrow, and the adjacent normal tissue measurement location, indicated by the left arrow. In Fig. 2(b), images of the back tumor and normal measurement sites are indicated by the left and the right arrows, respectively. The CT scans clearly show that for the 1.7–2.7-cm range of source–detector separations employed, FDPM data were primarily influenced by tumor and subcutaneous fat. Although the abdominal tumor had approximately a 1-cm-thick layer of skin and fat above it, this zone is likely to have been depleted by the time FDPM measurements were performed, because of rapid tumor growth during the 1-month interval between the CT scan and the FDPM measurement. The back tumor did not

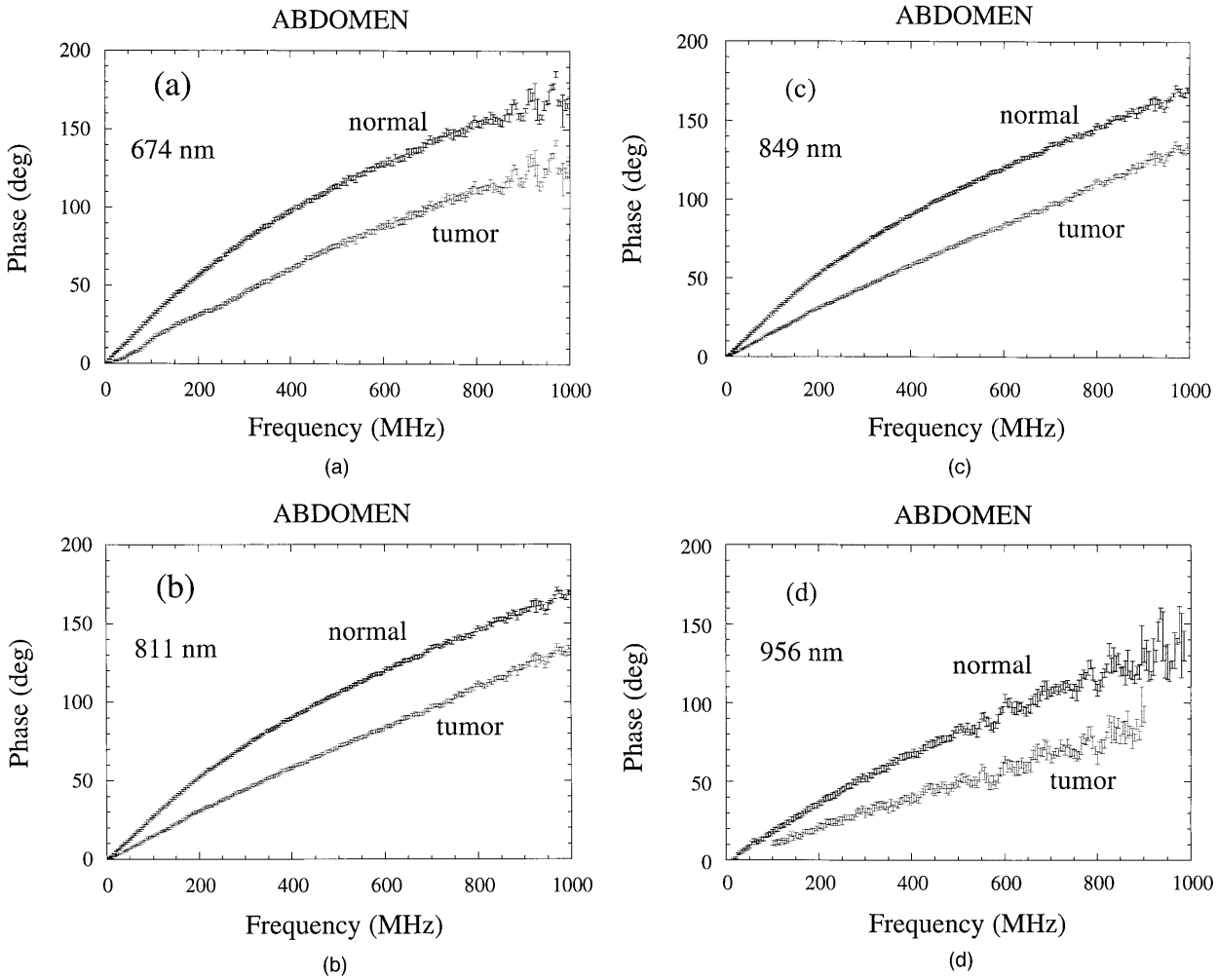

Fig. 3. (a) Phase shift versus FDPM data obtained on normal and malignant tissue on the human subject's abdomen. These phase-shift data were acquired at a distance of 1.7 cm from the light source at a wavelength of 674 nm. (b) Same as (a), except the source wavelength was 811 nm. (c) Same as (a), except the source wavelength was 849 nm. (d) Same as (a), except the source wavelength was 956 nm.

appear to have an appreciable layer of normal tissue above it. Of course, CT images do not necessarily reveal the exact zone of malignant tissue. Thus it is possible that the tumor optical property measurements may, to some extent, contain a small contribution from surrounding normal structures. However, we believe that this effect is probably minimal in view of the high tumor–normal tissue optical property contrast and the good agreement between the measurements of the stomach and back malignant sites (see Section 4).

The patient was breathing O_2 from a tank (through a nasal cannula at 2 L/min) before and throughout the duration of our FDPM measurements. All four of the diode laser sources currently available on our FDPM instrument were used in these measurements: 674, 811, 849, and 956 nm (average power coupled to the tissue surface was approximately 30 mW for the 674-, 811-, and 849-nm sources and approximately 1 mW for the 956-nm diode because of poor coupling of the optical fiber with the diode laser source). As described above, the source modulation frequencies ranged from 300 kHz to 1 GHz, and FDPM data were recorded in 5-MHz increments. Average phase shift $\Phi_{\text{measured}}(\mu_a, \mu_s', \rho, \omega)$ values were obtained over this ~1-GHz bandwidth by the performance of two multifrequency sweeps per measurement. The uncertainty in $\Phi_{\text{measured}}(\mu_a, \mu_s', \rho, \omega)$ is the standard deviation from this quantity (determined by the averaging of the deviations from this quantity over the total number of frequency sweeps). The uncertainty in $\Phi_{\text{measured}}(\mu_a, \mu_s', \rho, \omega)$ together with the uncertainty in $\Phi_{\text{instrument}}(\omega, \lambda)$ (which, as we mentioned above in Subsection 3.B, is determined by making a calibration measurement on a macroscopically homogeneous standard phantom) determines the magnitude of the error bars on the $\Phi_{\text{medium}}(\mu_a, \mu_s', \rho, \omega)$ data shown in Fig. 3. A handheld probe was used that accommodated several source–detector separations, ranging from 1.2 to 2.7 cm in 0.5-cm increments. The FDPM instrument was calibrated as described above by the performance of measurements at a fixed source–detector separation on a standard reference material.

Phase-shift data obtained from FDPM measurements on tissue [see $\Phi_{\text{medium}}(\mu_a, \mu_s', \rho, \omega)$ data, Fig. 3] were fit to Eq. (1) to extract the absolute optical absorption coefficient μ_a and the absolute optical reduced scattering coefficient μ_s' at a given λ and source–detector separation ρ. Each point of the phase shift versus frequency data fit to Eq. (1) was weighted in that fit according to the magnitude of its error bar. Minimization of the χ^2 surface in the fitting of the phase shift versus frequency data was obtained by the use of a Marquardt–Levenberg algorithm for minimizing χ^2 with respect to the fitting parameters μ_a and μ_s' in Eq. (1). A tissue refractive index of 1.40 was assumed in these data fits[15]; hence the value calculated for the effective reflection coefficient [see Eq. (7)] was $R_{\text{eff}} = 0.493$.[14]

We assume that the chomophores contributing to μ_a in the human subject are principally oxyhemoglobin, deoxyhemoglobin,[16] and H_2O. The concentration of each component in the tissue is determined from the FDPM measurements of μ_a at three different wavelengths. A system of three equations of the form

$$\epsilon^{\lambda}_{[\text{Hb}]}[\text{Hb}] + \epsilon^{\lambda}_{[\text{HbO}_2]}[\text{HbO}_2] + \epsilon^{\lambda}_{[\text{H}_2\text{O}]}[\text{H}_2\text{O}] = \mu_a^{\lambda} \quad (10)$$

is solved, where $\epsilon^{\lambda}_{[\text{chrom.}]}$ is the extinction coefficient (in units of square centimeters per mole) of a given chromophore at wavelength λ and [Hb], [HbO_2], and [H_2O] are, respectively, the concentration of Hb, oxygenated Hb, and H_2O (in units of mole per cubic centimeter) in the tissue under study. Because measurements of μ_a are made at four different light wavelengths, we use two different sets of three equations to determine the three unknown quantities [Hb], [HbO_2], and [H_2O]. $\epsilon^{\lambda}_{[\text{Hb}]}$, $\epsilon^{\lambda}_{[\text{HbO}_2]}$, and $\epsilon^{\lambda}_{[\text{H}_2\text{O}]}$ are obtained from literature values (note that we report these literature values in a natural logarithm scale).[17,18] For the wavelengths of 674, 811, and 956 nm, the matrix representation of the system of three equations given by Eq. (10) is

$$\begin{bmatrix} 6.5783 \times 10^6 & 0.7401 \times 10^6 & 0.0748 \\ 1.8331 \times 10^6 & 2.1539 \times 10^6 & 0.427 \\ 1.5006 \times 10^6 & 3.0486 \times 10^6 & 7.24 \end{bmatrix} \times \begin{pmatrix} [\text{Hb}] \\ [\text{HbO}_2] \\ [\text{H}_2\text{O}] \end{pmatrix} = \begin{pmatrix} \mu_a^{674} \\ \mu_a^{811} \\ \mu_a^{956} \end{pmatrix}. \quad (11)$$

Each column of the matrix in Eq. (11) contains the extinction coefficients of a given chromophore at each of the above-mentioned wavelengths. Each row of the matrix corresponds to a different light wavelength λ. Multiplication of the above equation by the inverse of the above matrix of extinction coefficients yields values for [Hb], [HbO_2], and [H_2O] in the tissue interrogated by our FPDM instrument. For the wavelengths of 674, 849, and 956 nm, the matrix representation of the system of three equations given by Eq. (10) is

$$\begin{bmatrix} 6.5783 \times 10^6 & 0.7401 \times 10^6 & 0.0748 \\ 1.8089 \times 10^6 & 2.6588 \times 10^6 & 0.781 \\ 1.5006 \times 10^6 & 3.0486 \times 10^6 & 7.24 \end{bmatrix} \times \begin{pmatrix} [\text{Hb}] \\ [\text{HbO}_2] \\ [\text{H}_2\text{O}] \end{pmatrix} = \begin{pmatrix} \mu_a^{674} \\ \mu_a^{849} \\ \mu_a^{956} \end{pmatrix}. \quad (12)$$

Given the comparable magnitude and relatively small values of $\epsilon^{\lambda}_{[\text{H}_2\text{O}]}$ at 811 and 849 nm (i.e., $\epsilon^{\lambda}_{[\text{H}_2\text{O}]}$ at 811 and 849 nm is more than a factor of 10^6 less than the Hb extinction coefficients $\epsilon^{\lambda}_{[\text{Hb}]}$ and $\epsilon^{\lambda}_{[\text{HbO}_2]}$ at 811 and 849 nm), we did not find it useful to use the 811- and 849-nm wavelengths together in our system of three equations and three unknowns to extract absolute concentration of [Hb], [HbO_2], and [H_2O] in the tissue. Rather, we found it preferable to include the μ_a value measured at only one or the other of these wavelengths with the 674- and 956-nm μ_a values in our system of three equations. This allowed for the simultaneous extraction of [Hb], [HbO_2], and [H_2O] concentration from our μ_a data. [Please refer to the above matrix Eqs. (11) and (12) for the $\epsilon^{\lambda}_{[\text{H}_2\text{O}]}$ values]. Confirmation of the validity of this approach is provided by our observation that the use of either 674- and 811-nm μ_a data, or 674- and 849-nm μ_a data in a system of (two equations)/(two unknowns) yields, within experimental uncertainties, the same result for [Hb] and [HbO_2]. We therefore stress that inclusion of the μ_a value determined at 956 nm into our system of three equations was essential for extracting absolute H_2O concentration from our *in vivo* tissue measurements.

Finally, for a system of equations of the form of Eq. (11) or Eq. (12), in which the 3×3 matrix in these equations is given as

$$\mathbf{M} \equiv \begin{bmatrix} a & b & c \\ d & e & f \\ g & h & i \end{bmatrix}, \quad (13)$$

the total uncertainties δ for each parameter [Hb], [HbO_2], and [H_2O] can be determined, i.e.,

$$\delta[\text{Hb}] = \frac{1}{\det(\mathbf{M})}\left[(\Delta\mu_a^{\lambda_1})^2(ei - hf)^2 + (\Delta\mu_a^{\lambda_2})^2 \times (bi - hc)^2 + (\Delta\mu_a^{\lambda_3})^2(bf - ec)^2\right]^{1/2}, \quad (14)$$

$$\delta[\text{HbO}_2] = \frac{1}{\det(\mathbf{M})}\left[(\Delta\mu_a^{\lambda_1})^2(di - fg)^2 + (\Delta\mu_a^{\lambda_2})^2 \times (ai - gc)^2 + (\Delta\mu_a^{\lambda_3})^2(af - dc)^2\right]^{1/2}, \quad (15)$$

$$\delta[\text{H}_2\text{O}] = \frac{1}{\det(\mathbf{M})}\left[(\Delta\mu_a^{\lambda_1})^2(dh - ge)^2 + (\Delta\mu_a^{\lambda_2})^2 \times (ah - gb)^2 + (\Delta\mu_a^{\lambda_3})^2(ae - db)^2\right]^{1/2}. \quad (16)$$

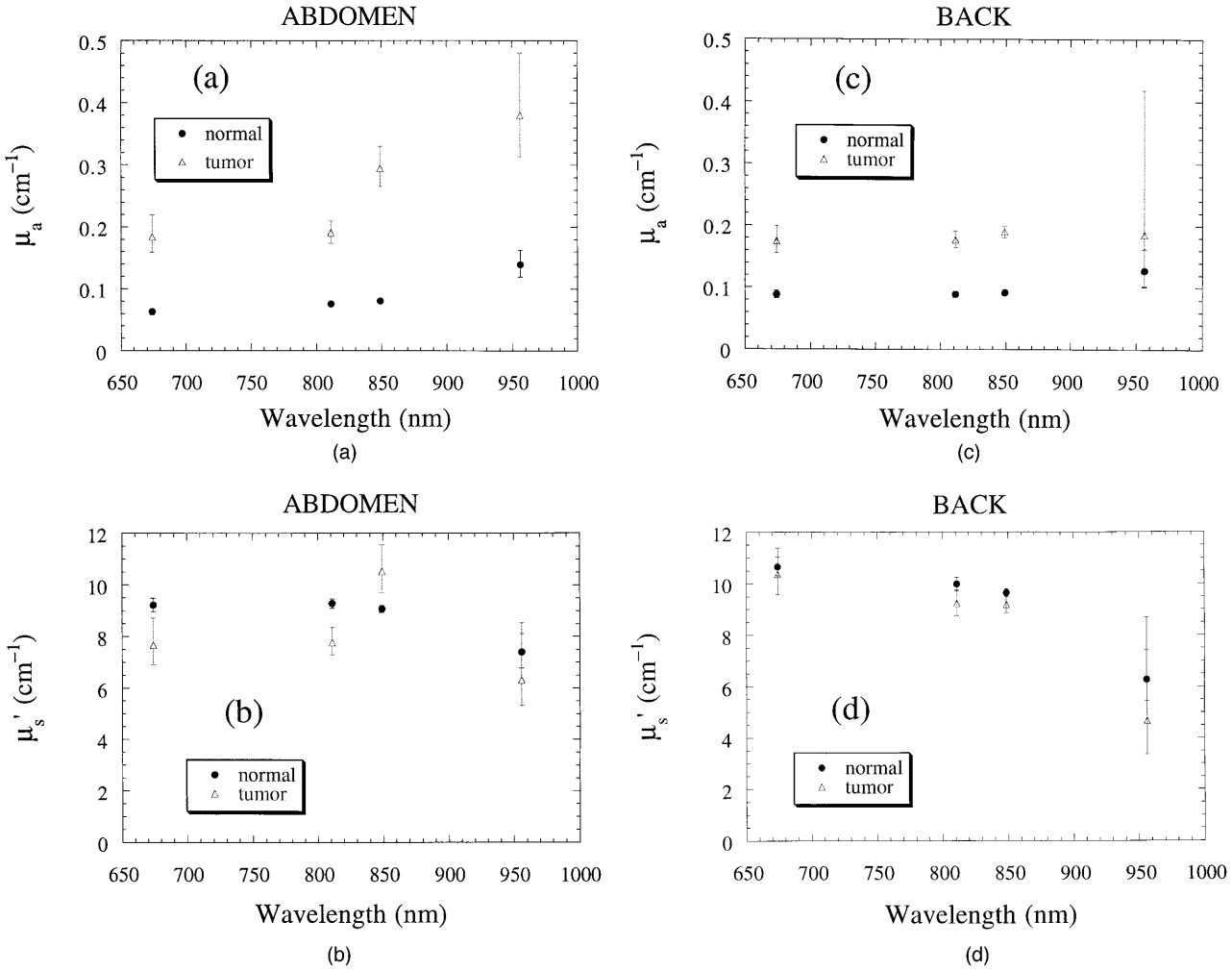

Fig. 4. (a) Absolute absorption coefficient μ_a versus source wavelength obtained for normal and malignant tissue on the human subject's abdomen. The μ_a values were extracted from best fits of Eq. (1) to the abdomen phase shift versus modulation frequency data (shown in Fig. 3). The source–detector separation was 1.7 cm. (b) Reduced scattering coefficient μ_s' versus source wavelength obtained for normal and malignant tissue on the human subject's abdomen. The μ_s' values were extracted from best fits of Eq. (1) to the abdomen phase shift versus modulation frequency data (shown in Fig. 3). The source–detector separation was 1.7 cm. (c) Same as (a), except that the μ_a values were obtained for normal and tumor tissue on the subject's back. The source–detector separation was 2.2 cm for these measurements. (d) Same as (b), except that the μ_s' values were obtained for normal and tumor tissue on the subject's back. The source–detector separation was 2.2 cm for these measurements.

4. Results and Discussion

Figure 3 compares the phase versus frequency response obtained on normal and malignant abdominal tissue. These phase-shift data were acquired at a 1.7-cm source–detector separation for four different wavelengths. Phase values have been corrected for $\Phi_{\text{instrument}}(\omega, \lambda)$, as described above, by the use of a standard reference material. The information presented in Fig. 3 is therefore entirely a consequence of the tissue optical properties, the source modulation frequency, and the 1.7-cm source–detector separation on the tissue surface. Note that at all wavelengths and modulation frequencies, the normal abdominal tissue phase lag is greater than that of the tumor. In addition, the normal tissue phase versus frequency response displays greater curvature than the tumor phase versus frequency data. Figure 3(d) data are relatively noisy because of the lower average optical power of the 956-nm diode laser (only 1-mW average power).

Figure 4 shows plots of μ_a and μ_s' values extracted from best fits of the abdomen phase shift versus modulation frequency data (shown in Fig. 3) and from best fits of phase shift versus frequency data (not shown) obtained from normal and malignant tissue on the human subject's back. The fitting expression is given by Eq. (1). The uncertainties shown for the μ_a and μ_s' values were estimated for each fit from the χ^2 distribution by the use of a 0.67 confidence interval. Tables 1 and 2 show the optical parameters μ_a and μ_s' extracted from the fits to all the phase-shift data acquired from the human subject's abdomen and back (both normal and malignant tissue) at all source–detector separations (i.e., 1.7, 2.2, and 2.7 cm)

Table 1. Summary of the Optical Parameters μ_a and μ_s' Extracted from the Best Fits to the Phase-Shift Data Acquired from the Human Subject's Normal Abdomen and Tumor Abdomen

		Normal Abdomen		Tumor Abdomen	
λ (nm)	ρ (cm)	μ_a (cm^{-1})	μ_s' (cm^{-1})	μ_a (cm^{-1})	μ_s' (cm^{-1})
674	1.7	0.0627 ± 0.0046	9.23 ± 0.26	$0.184^{+0.035}_{-0.025}$	$7.66^{+1.06}_{-0.75}$
811	1.7	0.0755 ± 0.0036	9.29 ± 0.18	$0.190^{+0.020}_{-0.017}$	$7.78^{+0.58}_{-0.47}$
849	1.7	0.0801 ± 0.0030	9.07 ± 0.14	$0.294^{+0.036}_{-0.029}$	$10.5^{+1.1}_{-0.8}$
956	1.7	$0.139^{+0.024}_{-0.020}$	$7.39^{+0.72}_{-0.61}$	$0.380^{+0.100}_{-0.066}$	$6.3^{+2.2}_{-1.0}$
674	2.2	0.0589 ± 0.0036	8.94 ± 0.19	$0.169^{+0.023}_{-0.018}$	$8.48^{+0.83}_{-0.63}$
811	2.2	$0.0645 + 0.0032$	8.82 ± 0.18	$0.190^{+0.016}_{-0.014}$	$8.30^{+0.53}_{-0.45}$
849	2.2	0.0690 ± 0.0025	8.77 ± 0.14	$0.276^{+0.033}_{-0.026}$	$9.93^{+0.97}_{-0.77}$
956	2.2	$0.111^{+0.016}_{-0.013}$	$7.00^{+0.70}_{-0.55}$	—	—
674	2.7	$0.0583^{+0.0085}_{-0.0055}$	$9.16^{+0.24}_{-0.35}$	$0.168^{+0.020}_{-0.016}$	$8.22^{+0.72}_{-0.56}$
811	2.7	0.0626 ± 0.0030	9.11 ± 0.15	$0.214^{+0.019}_{-0.016}$	$8.55^{+0.65}_{-0.50}$
849	2.7	0.0696 ± 0.0030	9.03 ± 0.15	$0.227^{+0.021}_{-0.018}$	$8.14^{+0.59}_{-0.51}$
956	2.7	0.107 ± 0.010	$6.97^{+0.70}_{-0.50}$	—	—

ρ and at each wavelength λ. These results confirm significant absorption differences between normal and tumor tissue at all wavelengths. Scattering changes are less significant, but exhibit consistent wavelength-dependent behavior. Lower tumor scattering parameters (versus normal tissue) may be due to a loss of cellularity and increased H_2O content of necrotic zones. This could diminish both the density and the efficiency of available scatterers. Consequently we expect that μ_s' measurements may be more sensitive to early-stage highly cellular tumors.

Figure 5 shows quantitative bar graphs of *in vivo* physiological properties of the human subject's normal and malignant abdominal tissue calculated by the use of combinations of μ_a values obtained at three different wavelengths [see Eqs. (11) and (12)]. The

Table 2. Summary of the Optical Parameters μ_a and μ_s' Extracted from the Best Fits to the Phase-Shift Data Acquired from the Human Subject's Normal Back and Tumor Back[a]

	Normal Back		Tumor Back	
λ (nm)	μ_a (cm^{-1})	μ_s' (cm^{-1})	μ_a (cm^{-1})	μ_s' (cm^{-1})
674	$0.0883^{+0.0063}_{-0.0058}$	10.7 ± 0.4	$0.174^{+0.024}_{-0.019}$	$10.4^{+1.0}_{-0.8}$
811	0.0892 ± 0.0050	9.99 ± 0.27	$0.177^{+0.014}_{-0.012}$	$9.23^{+0.53}_{-0.47}$
849	0.0915 ± 0.0030	9.65 ± 0.15	0.190 ± 0.010	$9.20^{+0.34}_{-0.32}$
956	$0.127^{+0.035}_{-0.026}$	$6.3^{+1.1}_{-0.8}$	$0.186^{+0.233}_{-0.083}$	$4.7^{+4.0}_{-1.3}$

[a]For all measurements in this table, $\rho = 2.2$ cm.

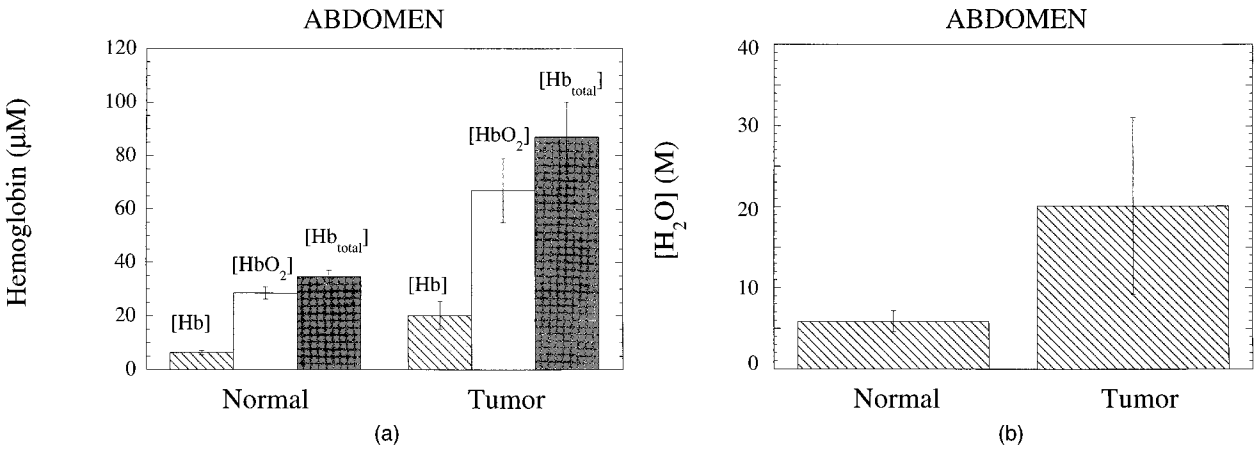

Fig. 5. (a) Hb concentrations (deoxyhemoglobin, oxyhemoglobin, and total) for normal and tumor locations on a human abdomen that are calculated from wavelength-dependent μ_a values [refer to matrix Eqs. (11) and (12) for calculation method], (b) H_2O concentrations for normal and tumor locations on human abdomen that are calculated from wavelength-dependent μ_a values [refer to matrix Eqs. (11) and (12) for calculation method].

μ_a values used to generate the numbers shown in Fig. 5 were extracted from the best fits of our phase data acquired at a 1.7-cm source–detector separation. The in vivo physiological parameters displayed in Figs. 5(a) and 5(b) are, respectively, deoxygenated and oxygenated Hb concentrations (i.e., [Hb] and [HbO_2], in units of millimolar concentration) and H_2O concentration ([H_2O] in units of molar concentration). The combinations of μ_a values used in our calculations of [Hb], [HbO_2], and [H_2O] were chosen to minimize the uncertainty in these parameters that we calculated from Eqs. (14)–(16). For the reasons already given above in Subsection 3.C., we did not find it useful to use the μ_a values acquired at 811 and 849 nm together in the system of three equations given by Eq. (10). We believe that the best way to reduce the uncertainty in the H_2O concentration extracted from our data will be to improve the precision of the μ_a values acquired at 956 nm. Improvement in the signal-to-noise ratio of our measurements at 956 nm by an increase in the optical power coupled to the tissue should be useful in improving the precision with which we may determine μ_a and hence absolute H_2O concentration in future *in vivo* measurements. The average power of the 956-nm light coupled to the tissue in the measurements presented here can be increased from 1 to approximately 30 mW. Figure 5(a) shows that both [Hb] and [HbO_2] (and hence total Hb concentration) in the abdominal tumor tissue were approximately double that of the normal abdominal tissue. Figure 5(b) shows the abdominal tumor tissue to have a higher H_2O concentration than the normal abdominal tissue, although it must be noted that the error on the abdominal tumor tissue H_2O concentration is large because of the large uncertainty in μ_a^{956} used in the calculation of this quantity [see Fig. 4(a) and the columns under Tumor Abdomen in Table 1. Although the relative values of [H_2O] are probably correct, it is important to point out that the accuracy of the absolute [H_2O] quantity is not easy to estimate. This is because we determined [H_2O] from $\epsilon^{\lambda}_{[H2O]}$ values measured in pure systems.[17] Although these are probably the most accurate H_2O extinction coefficients available, they may not be exact for biological systems in which H_2O is found in a variety of states (e.g., protein bound, free) that can have an impact on $\epsilon^{\lambda}_{[H_2O]}$.

Table 3 shows the results of the calculation of [Hb], [HbO_2], and [H_2O] by the use of μ_a values measured at given source–detector separations ρ on the abdomen and the back (both normal and malignant tissue). In cases in which the phase-shift data

Table 3. Summary of Physiological Parameters for Normal and Tumor Locations on a Human Abdomen and Back Calculated from Wavelength-Dependent Optical Absorption Coefficients given in Tables 1 and 2[a]

Location	ρ (cm)	[Hb] (μM)	[HbO_2] (μM)	[H_2O] (M)	[Hb_{total}] (μM)	% Oxygenation
Normal abdomen	1.7	6.25 ± 0.82	28.6 ± 2.2	5.87 ± 1.31	34.8 ± 2.3	82.2 ± 8.3
	2.2	6.22 ± 0.64	23.9 ± 1.9	4.00 ± 2.23	30.1 ± 2.0	79.4 ± 8.2
	2.7	6.23 ± 1.19	23.0 ± 2.1	3.95 ± 1.94	29.2 ± 2.4	78.8 ± 9.7
Tumor abdomen	1.7	20.2 ± 5.2	67 ± 12	20.1 ± 10.8	87 ± 13	77 ± 18
	2.2	17.4 ± 3.6	73.4 ± 8.3	N/A	90.8 ± 9.0	81 ± 12
	2.7	15.9 ± 3.2	86.0 ± 9.6	N/A	102 ± 10	84 ± 13
Normal back	2.2	9.68 ± 1.04	33.2 ± 2.7	N/A	42.9 ± 2.9	77.4 ± 8.2
Tumor back	2.2	19.1 ± 3.7	66.0 ± 7.4	N/A	85.1 ± 8.2	78 ± 12

[a]Refer to matrix Eqs. (11) and (12) for calculation method.

acquired at 956 nm was too poor to determine μ_a^{956} precisely, we were unable to calculate tissue H_2O concentration. Under these conditions, measurements of μ_a at two wavelengths, e.g., μ_a^{674} and μ_a^{811} or μ_a^{674} and μ_a^{849}, were used to calculate the [Hb] and [HbO_2].

The BVF range in the subject's normal abdominal tissue is derived from the [Hb_{total}] values given in Table 3 and hemotologic values obtained when blood was drawn from the subject on the day of the optical FDPM measurements. The subject's hemotologic values obtained from his drawn blood were 318 g Hb_{total}/(L of erythrocytes) and a hematocrit (red blood cell volume/blood volume) of 33.6%. Given that Hb_{total} molecular weight is 64.5×10^3 g/mole,[19] the concentration of Hb in the subject's whole blood was approximately (318 g/L) $\times$ 0.336/(64.5×10^3 g/mole) = 1.66×10^3 μM Hb_{total} on the day of the FDPM measurements. Because [Hb_{total}] values measured by FDPM in the subject's normal abdominal tissue ranged from 29.2 to 34.8 μM, we obtain a tissue BVF of (29.2 to 34.8 μM)/(1.66×10^3 μM) $\times$ 100 = 1.8%–2.1% in the subject's normal abdominal tissue. Given that the [Hb_{total}] values we measured by FDPM in the subject's abdominal tumor tissue range from 87 to 102 μM, we obtain a (87 to 102 μM)/(1.66×10^3 μM) = 5.2%–6.1% BVF range in the subject's abdominal tumor tissue. This is a factor of ~3 greater than measured normal abdominal tissue BVF.

The H_2O volume fraction in the subject's normal abdominal tissue is derived from the [H_2O] values given in Table 3. Given that the molecular weight of water is 18 g/mole and the density of water is 1000 g/L, the concentration of water is approximately (1000 g/L)/(18 g/mole) = 55.6 M. The [H_2O] values we measured by FDPM in the subject's normal abdominal tissue range from 3.95 to 5.87 M; hence we obtain a H_2O volume fraction range of (3.95 to 5.87 μM)/(55.6 M) $\times$ 100 = 7.1%–10.6% in the subject's normal abdominal tissue. This is comparable with the lower end of the 11.4%–30.5% range given in the literature for H_2O percentage in human fatty adipose tissue.[20] Abdominal tumor tissue H_2O percentage ranged from 16% to 56%, or roughly twofold–fivefold higher than that of normal abdominal tissue.

These values neglect the possibility that fat absorption contributes to μ_a^{956}. In practical terms, fat absorption is difficult to quantify and is, at the wavelengths used in this study, less significant than other tissue components. Nevertheless, H_2O concentration measurements of normal, adipose-dominated abdominal and back tissues may be artificially elevated because of an underestimation on our part of fat absorption to our measured values of μ_a^{956}. Of course, if this were the case, it would provide even further evidence of contrast between normal and malignant tissues. In any event, H_2O contrast is likely to be primarily a reflection of differences in tumor versus normal tissue vascularity (i.e., BVF) rather than intrinsic variations in tissue H_2O content. Other possible sources of H_2O concentration variations include increased fluid retention as indicated by elevated tumor interstitial fluid pressure levels.[21]

5. Conclusion

Overall, optical property data from normal and malignant sites are remarkably consistent. FDPM measurements sample a combination of necrotic core and high blood volume cortex tumor regions. Regardless of the precise locations probed, we have observed that total Hb (which is proportional to blood volume) and H_2O content are of the order of twofold–fivefold higher in tumor versus normal tissue. Scattering spectra suggest smaller, but detectable, differences in wavelength-dependent behavior between tissue types. Although these preliminary data were not recorded from breast tissues, we believe that these definitive results obtained from adenocarcinoma lesions growing in host adipose tissue (i.e., comparable with breast disease) suggest that FDPM will have utility in breast cancer diagnostics.

We are grateful to Harold Fry for his generous contribution to these studies. This work was made possible, in part, through access to the Laser Microbeam and Medical Program and the Clinical Cancer Center Optical Biology Shared Resource at the University of California at Irvine. These facilities are supported by the U.S. National Institutes of Health under grants RR-01192 and CA-62203, respectively. Beckman Laser Institute programmatic support was provided by the U.S. Department of Energy (DOE DE-FG03-91ER61227) and the U.S. Office of Naval Research (ONR N00014-91-C-0134). O. Coquoz acknowledges the Swiss National Science Foundation and the Cancer Research Switzerland (BIL KFS 205-9-1995). B. J. Tromberg acknowledges the U.S. National Institutes of Health (GM50958), the Whitaker Foundation (WF16493), and Beckman Instruments, Inc.

References

1. W. F. Cheong, S. A. Prahl, and A. J. Welch, "A review of the optical properties of biological tissues," IEEE J. Quantum Electron. **26,** 2166–2185 (1990).
2. V. G. Peters, D. R. Wyman, M. S. Patterson, and G. L. Frank, "Optical properties of normal and diseased human breast tissues in the visible and near infrared," Phys. Med. Biol. **335,** 1317–1334 (1990).
3. T. L. Troy, D. L. Page, and E. M. Sevick-Muraca "Optical properties of normal and diseased breast tissue," in OSA Trends in Optics and Photonics, Vol. 3, *Biomedical Optical Spectroscopy and Diagnostics*, E. Sevick-Muraca and D. Benaron, eds. (Optical Society of America, Washington, D.C., 1996), pp. 59–61.
4. B. J. Tromberg, R. C. Haskell, S. J. Madsen, and L. O. Svaasand, "Characterization of tissue optical properties using photon density waves," Comments Mol. Cell. Biophys. **8,** 359–386 (1996).
5. S. J. Madsen, E. R. Anderson, R. C. Haskell, and B. J. Tromberg, "Portable high-bandwidth frequency-domain photon migration instrument for tissue spectroscopy," Opt. Lett. **19,** 1934–1936 (1994).
6. J. B. Fishkin and E. Gratton, "Propagation of photon density

waves in strongly scattering media containing an absorbing semi-infinite plane bounded by a straight edge," J. Opt. Soc. Am. A **10,** 127–140 (1993).
7. M. A. O'Leary, D. A. Boas, B. Chance, and A. G. Yodh, "Refraction of diffuse photon density waves," Phys. Rev. Lett. **69,** 2658–2661 (1992).
8. D. A. Boas, M. A. O'Leary, B. Chance, and A. G. Yodh, "Scattering and wavelength transduction of diffuse photon density waves," Phys. Rev. E **47,** R2999–R3002 (1993).
9. B. J. Tromberg, L. O. Svaasand, T. Tsay, and R. C. Haskell, "Properties of photon density waves in multiple-scattering media," Appl. Opt. **32,** 607–616 (1993).
10. J. B. Fishkin, P. T. C. So, A. E. Cerussi, S. Fantini, M. A. Franceschini, and E. Gratton, "Frequency-domain method for measuring spectral properties in multiple-scattering media: methemoglobin absorption spectrum in a tissuelike phantom," Appl. Optics **34,** 1143–1155 (1995).
11. S. Fantini, M. A. Franceschini, J. B. Fishkin, B. Barbieri, and E. Gratton, "Quantitative determination of the absorption spectra of chromophores in strongly scattering media: a light-emitting-diode-based technique," Appl. Opt. **33,** 5204–5213 (1994).
12. M. S. Patterson, J. D. Moulton, B. C. Wilson, K. W. Berndt, and J. R. Lakowicz, "Frequency-domain reflectance for the determination of the scattering and absorption properties of tissue," Appl. Opt. **30,** 4474–4476 (1991).
13. J. B. Fishkin, S. Fantini, M. J. vandeVen, and E. Gratton, "Gigahertz photon density waves in a turbid medium: theory and experiments," Phys. Rev. E **53,** 2307–2319 (1996).
14. R. C. Haskell, L. O. Svaasand, T.-T. Tsay, T.-C. Feng, M. S. McAdams, and B. J. Tromberg, "Boundary conditions for the diffusion equation in radiative transfer," J. Opt. Soc. Am. A **11,** 2727–2741 (1994).
15. F. P. Bolin, L. E. Preuss, R. C. Taylor, and R. J. Ference, "Refractive index of some mammalian tissues using a fiber optic cladding method," Appl. Opt. **28,** 2297–2303 (1989).
16. E. M. Sevick, B. Chance, J. Leigh, S. Nioka, and M. Maris, "Quantitation of time- and frequency-resolved optical spectra for the determination of tissue oxygenation," Anal. Biochem. **195,** 330–351 (1991).
17. G. M. Hale and M. R. Querry, "Optical constants of water in the 200 nm to 200 m wavelength region," Appl. Opt. **12,** 555–563 (1973).
18. M. Cope, "The development of a near infrared spectroscopy system and its application for non invasive monitoring of cerebral blood and tissue oxygenation in the newborn infant," Ph.D. dissertation (Department of Medical Physics and Bioengineering, University of London, University College London, UK, 1991).
19. A. C. Guyton, *Textbook of Medical Physiology* (Saunders, Philadelphia, Pa., 1991), p. 360.
20. F. A. Duck, *Physical Properties of Tissue* (Academic, London, 1990), p. 320.
21. R. A. Zlotecki, L. T. Baxter, Y. Boucher, and R. K. Jain, "Pharmacologic modification of tumor blood flow and interstitial fluid pressure in a human tumor xenograft: network analysis and mechanistic interpretation," Microvasc. Res. **50,** 429–443 (1995).